Mechatronics 24 (2014) 724–733

Contents lists available at ScienceDirect

Mechatronics

journal homepage: www.elsevier.com/locate/mechatronics

# High-bandwidth tracking control of piezo-actuated nanopositioning stages using closed-loop input shaper

Mei-Ju Yang, Guo-Ying Gu, Li-Min Zhu *

*State Key Laboratory of Mechanical System and Vibration, School of Mechanical Engineering, Shanghai Jiao Tong University, Shanghai 200240, China*

ARTICLE INFO

*Article history:*
Received 29 June 2013
Revised 23 February 2014
Accepted 28 February 2014
Available online 27 March 2014

*Keywords:*
Nanopositioning stages
Piezoelectric actuators
Tracking control
Closed-loop input shaper
Hysteresis compensation

ABSTRACT

An integrated control strategy for piezo-actuated nanopositioning stages is proposed in this paper. The aim is to achieve high-speed and high-precision tracking control of nanopositioning stages. For this purpose, a direct inverse compensation method is firstly applied to eliminate the hysteresis nonlinearity without involving inverse model calculation. Then, an inside-the-loop input shaper is designed to suppress the vibration of the compensated system. A Smith predictor is introduced to prevent the potential closed-loop instability caused by the time delay of the inside-the-loop input shaper. Finally, a high-gain feedback controller is employed to handle the disturbances and modeling errors. To demonstrate the effectiveness of the proposed control method, comparative experiments are carried out on a piezoelectric actuated stage. The results show that the proposed control approach increases the tracking bandwidth of the stage from 22.6 Hz to 510 Hz.



## 1. Introduction

Nanopositioning stages are widely used in high-precision positioning and tracking applications, e.g., scanning probe microscopy [1], ultra-precision machine tools [2], and micromanipulator [3]. Most of these stages utilize piezoelectric actuators for actuation due to the excellent advantages of fast response time, high positioning precision, large output force, high stiffness, and small size. However, there are two factors limiting the speed and accuracy of the nanopositioning stage. One is the lightly damped resonances due to the mechanical dynamics, and the other is the inherent hysteresis nonlinearity of the piezoelectric material.

In order to achieve high bandwidth control of nanopositioning stages, many efforts have been made by the researchers to deal with the problem of the lightly damped resonances. One way to increase the operating speed is to build a piezo-actuated stage that is sufficiently stiff and lightweight [3]. A disadvantage of this approach is that its maximum traversal range is limited to a few microns. Furthermore, the operating frequency is still limited by the resonance frequency. Therefore, development of control techniques to suppress the vibrations becomes popular. Many damping control strategies are developed in the literature, such as the notch filter [4], input shaping [5–7], integral resonant control [8], and positive position feedback [9]. The input shaping control has been demonstrated as a simple and effective means to suppress the unwanted vibrations, and widely used in many applications, such as piezoelectric actuator [10,11], flexible manipulator [6,12–15], flexible spacecraft [16–18], and cranes [19,20]. The traditional input shaper is usually put in the forward path of the closed-loop system, which can be considered as a smart filter of the reference signal. However, this standard feedforward configuration does not have any impact on the control system response to immeasurable disturbances, noises, and uncertainty. In order to reduce this sensitivity effect, different kinds of closed-loop input shaping controllers were developed in the literature [21–26]. Kapila et al. designed a standard input shaper in conjunction with a full-state feedback controller to perform well despite of modeling errors in the timing of the impulses. [21]. Huey et al. developed a closed-loop input shaper [22,23]. They discussed the closed-loop stability utilizing input shapers inside the loop. They also investigated some useful applications of closed-loop input shaper. Using a structure already known from Internal Model Control, Staehlin and Singh transformed the outside-the-loop input shaper to the closed-loop input shaping controller [24]. Hung proposed a feedback input shaping configuration, which puts the input shaper within feedback loops [25]. This configuration takes advantage of the superior damping qualities of the input shaper, while reducing parametric sensitivity and uncertainty through the feedback controller. However, the main drawback of this approach is the existence of the time delays in feedback loops. It not only presents

* Corresponding author. Tel.: +86 21 34206545; fax: +86 21 34206086.
*E-mail addresses:* yangmeixianglian@sjtu.edu.cn (M.-J. Yang), guguoying@sjtu.edu.cn (G.-Y. Gu), zhulm@sjtu.edu.cn (L.-M. Zhu).

http://dx.doi.org/10.1016/j.mechatronics.2014.02.014
0957-4158/

a potential closed-loop instability, but also increases the implementation complexity of the linear control methods because of the irrational transfer function of the input shaper. Recently, a closed-loop input shaper based on the Smith predictor has been demonstrated as an effective means to prevent the instability issue due to the time delays in feedback loops. This technique has been successfully applied to damp the resonance mode of flexible beams [26].

It is worthy mentioning that the previous damping controllers are based on a linear description of the system, but the damping capabilities of the system can be greatly improved by considering the nonlinear phenomena present in the system. There are three main strategies for compensating hysteresis in piezoelectric actuators: charge control, feedback control, and feedforward control. The charge control [27] is based on the fact that the relationship between the displacement of piezo actuators and applied charge is nearly linear. However, this technique always increases the cost due to the requirement of charge amplifiers. The feedback control [28] is to reduce the hysteresis effect directly by feedback controller, where the hysteresis is considered as disturbance. However, in this category, a sophisticated control algorithm is generally required, such as $H_\infty$ control, sliding model control, and robust adaptive control. Furthermore, due to nonsmooth and nonlinear behaviors of the hysteresis, the main difficulty for such feedback control techniques lies in the stability analysis of the whole closed-loop system. The feedforward control is the most widely used approach to reduce the hysteresis effect when actuated by voltage input. It generally consists of modeling the real hysteresis nonlinearity, identifying the model parameters to match the real hysteresis and constructing an inverse model as a desired compensator. A number of hysteresis models are available in the literature to describe the hysteresis nonlinearity, such as the Bouc-Wen model [29], Prandtl-Ishlinskii model [30,31], and Preisach model [32]. The challenges of this technique are the modeling complexity and lack of robustness to model uncertainty.

In this paper, an integrated strategy is proposed to achieve high bandwidth tracking control of the piezo-actuated nanopositioning stage. The control scheme is composed of three components: (1) a hysteresis compensator which effectively cancels the nonlinear hysteresis of the piezoelectric actuators; (2) a closed-loop input shaper including an inside-the-loop input shaper and a Smith predictor for vibration damping control of the stage; and (3) a feedback controller to handle the disturbances and modeling errors. Note that the closed-loop input shaper is not actually closed itself; it just means that it is included in the feedback loop, distinguishing itself from the commonly used open-loop input shaper. The proposed integrated controller is implemented and demonstrated to perform well in reference tracking and disturbance rejection on a piezo-actuated nanopositioning stage. To the best knowledge of the authors, this work is the first attempt at introducing the closed-loop input shaper to the domain of high speed and high precision control of the piezo-actuated nanopositioning stages. The contributions of this work are threefold:

1. Different from the common hysteresis compensation approaches, a direct inverse hysteresis model is constructed from the experimental data. Both the hysteresis modeling and its complex inversion calculation are avoided, and therefore the computation complexity is reduced significantly.
2. The input shaper used in this work is placed inside the feedback loop for vibration damping control. Compared with the traditional outside-the-loop input shaper, the inside-the-loop input shaper can not only eliminate the vibration induced by the reference, but also has the potential of disturbance rejection. By placing the input shaper in the closed loop, it is capable of reducing oscillations caused by both the input and the output disturbances without overly slowing the closed-loop system by increasing the closed-loop damping ratio. Furthermore, the inside-the-loop input shaper allows the use of higher gains in the feedback control laws.
3. The Smith predictor is introduced to prevent the potential closed-loop instability due to the existence of time delays in the feedback loop.

The rest of the paper is organized as follows. Section 2 describes the principle of the control strategy. The implementation of the controller on a piezo-actuated nanopositioning stage is presented in Section 3. Section 4 summarizes and discusses the experimental results, and Section 5 concludes the paper.

## 2. Control schemes

In this section, the integrated strategy for vibration damping and tracking control of piezo-actuated nanopositionig stages are proposed. In the following, the development of the individual components will be expressed in detail.

### 2.1. Hysteresis compensator

The hysteresis of the piezoelectric actuator is an inherent multi-valued nonlinearity with the asymmetric characteristic. In order to linearize the system, the hysteresis compensation is necessary. A common strategy on hysteresis compensation consists of modeling the real hysteresis nonlinearity, identifying the model parameters to match the real hysteresis and constructing an inverse model as a desired compensator. Different from the commonly used strategies, a direct inverse hysteresis compensation method proposed in our previous work [33] is utilized in this work, which compensates for the hysteresis nonlinearity by constructing an inverse hysteresis model directly from the experimental data. By this way, both the hysteresis modeling and its complex inversion calculation are avoided.

The block diagram of the hysteresis compensation is illustrated in Fig. 1. For a given desired trajectory, denoted as $y_d(t)$, the inverse hysteresis model will generate an input signal $v(t)$ which is applied to the piezoelectric actuator; the output of the piezoelectric actuator is denoted as $y(t)$. The model of the piezoelectric actuator is considered as a cascade of a rate-independent hysteresis submodel $H$ and a linear dynamic submodel $G$ [34]. When the input signal $v(t)$ is composed of low-frequency components, the system dynamic $G$ is negligible. Hence, the output of the hysteresis model $w(t)$ is approximately equal to $y(t)$. If the inverse hysteresis model is ideal, the output $y(t)$ should follow the desired trajectory $y_d(t)$, that is $y(t) = y_d(t)$. Therefore, the input–output relationship of the inverse hysteresis model can be directly obtained by plotting $v(t)$ against $y(t)$, whereas the hysteresis model is obtained by plotting $y(t)$ against $v(t)$ as shown in Fig. 2. It can be observed that the inverse hysteresis loops and the hysteresis loops are symmetrical about the 45° line. Thus, the inverse hysteresis model can be directly derived from the experimental data just like the hysteresis

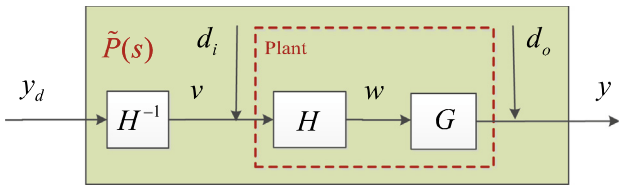


**Fig. 1.** The block diagram of hysteresis compensation.

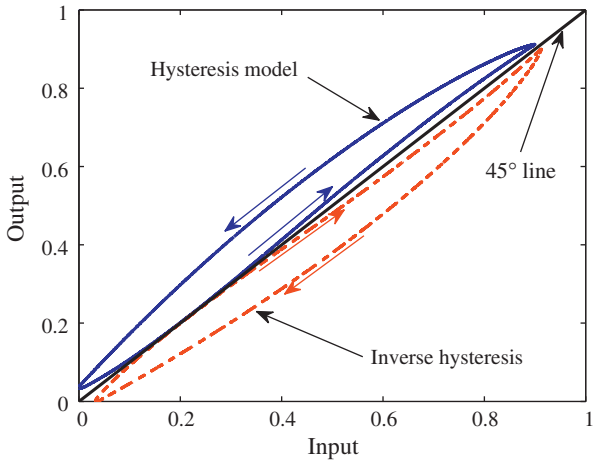


**Fig. 2.** Relationship between the hysteresis model and its inverse model.

modeling. Any of the hysteresis models can be used to describe the input–output relationship of the inverse hysteresis.

The Prandtl-Ishlinskii (P-I) model is one of the most widely used models to describe the hysteresis nonlinearity due to its simplicity and analytical inversion [30]. In this paper, it is chosen to construct the inverse hysteresis model. Considering the asymmetric hysteresis nonlinearity of the piezoelectric actuator, a modified Prandtl-Ishlinskii (MPI) model proposed in our previous work [31] is employed, which is defined in terms of weighted play operators and a polynomial input function as follows:

$$v(t) = g(y_d(t)) + \int_0^R p(r)F_r[y_d](t)dr \tag{1}$$

where $g(y_d(t)) = a_1 y_d^3(t) + a_2 y_d(t)$ is a polynomial input function with constants $a_1$ and $a_2$, $p(r)$ is a density function that is generally calculated from the experimental data, and $F_r[y_d](t)$ is a one-side play operator expressed as

$$\begin{aligned} F_r[y_d](0) &= \max\{y_d(0) - r, \min\{y_d(0), 0\}\} \\ F_r[y_d](t) &= \max\{y_d(t) - r, \min\{y_d(t), F_r[y_d](t - T)\}\} \end{aligned} \tag{2}$$

where $r$ is the input threshold of the play operators, and $T$ is the sampling period.

A discrete form is used to conveniently implement the real-time inverse hysteresis model as follows:

$$v(t) = a_1 y_d^3(t) + a_2 y_d(t) + \sum_{i=1}^{N} p_i F_{r_i}[y_d](t) \tag{3}$$

where $p_i$ denotes the weighting value of the play operator with the threshold value $r_i$, and $N$ is the number of the play operators. The parameters of this model can be identified with a modified particle swarm optimization [35]. The identified inverse hysteresis model is directly put in the feedforward path of the plant to cancel the hysteresis without the complex inversion calculation.

### 2.2. Input shaper

The input shaper is an effective control technique for reducing the unwanted vibrations of the damping system [36]. Most of the input shaper and feedback control combinations have utilized the input shaper outside of the loop. However, this typical configuration can only deal with the vibrations caused by the reference signals. It has no effect on the vibrations resulted from immeasurable disturbances and noises [23,26]. In order to solve this problem, the closed-loop input shaper is employed, which puts the input shaper within feedback loops [25]. A typical structure of

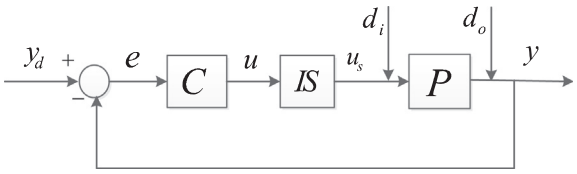


**Fig. 3.** The block diagram of feedback input shaping configuration.

the feedback input shaping configuration for a linear dynamic system $P$ is shown in Fig. 3, where $IS$ and $C$ represent the input shaper and feedback controller, respectively.

The input shaping process can be illustrated by time-delay blocks as shown in Fig. 4, where $A_i$ and $t_i$ are the amplitude and time location of the impulse $i$ respectively, and $n$ is the number of the impulses. Basically, both the positive and negative type of input shaper can be used for vibration suppression. In this work, for simplicity, the most common and simplest Zero-Vibration (ZV) input shaper with positive amplitudes [6,7,36,37] is employed, which contains two impulses. The design objectives are to determine the amplitudes $(A_1, A_2)$ and time locations $(t_1, t_2)$ of the impulses to achieve a zero residual vibration. Without loss of generality, we can set the time location of the first impulse equal to zero, that is $t_1 = 0$. The other parameters can be obtained by solving the following problem:

$$\begin{cases} A_1 + A_2 e^{\zeta\omega_n t_2}\cos(\omega_d t_2) = 0 \\ A_2 e^{\zeta\omega_n t_2}\sin(\omega_d t_2) = 0 \\ A_1 + A_2 = 1 \\ A_i > 0, i = 1, 2 \end{cases} \tag{4}$$

where $\omega_n$ and $\zeta$ represent the natural frequency and damping ratio of the system respectively, and $\omega_d = \omega_n\sqrt{1-\zeta^2}$ is the damped frequency. Defining $K = e^{\frac{-\zeta\pi}{\sqrt{1-\zeta^2}}}$, the parameters of the ZV input shaper can be expressed as:

$$\begin{bmatrix} A_i \\ t_i \end{bmatrix} = \begin{bmatrix} \frac{1}{1+K} & \frac{K}{1+K} \\ 0 & \frac{\pi}{\omega_d} \end{bmatrix} \tag{5}$$

Therefore, the ZV input shaper can be denoted in the Laplace domain as:

$$IS = A_1 + A_2 e^{-st_2} \tag{6}$$

where $s$ is the Laplace variable. The reader may refer to [36,37] for detailed discussions. To handle multiple vibration modes, an impulse sequence for each vibration mode can be designed independently. Then the impulse sequences can be convoluted together to form a sequence of impulses that attenuates vibration at multiple modes.

**Remark 1.** There are essential differences between the input shaper and notch filter [38]. First, the design of the input shaper is based on decaying sinusoids rather than the frequency domain techniques used for notch filter. In other words, notch filter

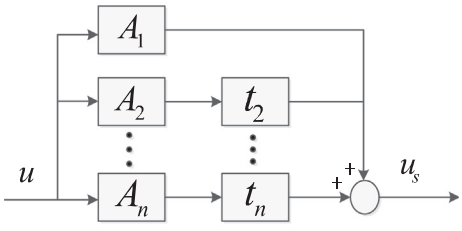


**Fig. 4.** Time-delay blocks representing input shaping.

removes a range of frequencies, while the input shaper removes a range of decaying sinusoids. Second, the input shaper offers a shorter rise time and lower level of residual vibration than the notch filter, even in the presence of modeling errors.

From the above discussion, the traditional input shaper, such as the ZV input shaper, only applies to the linear dynamic system. It cannot work well on piezo-actuated stages when the hysteresis nonlinearity exists. Thus, it is necessary to implement the hysteresis compensation to obtain an approximated linear dynamic system as shown in Fig. 1. Combining Figs. 1 and 3, the feedback input shaping configuration for piezo-actuated stages with hysteresis compensation is obtained as shown in Fig. 5, where $\tilde{P}(s)$ is the hysteresis compensated system, $IS$ is the input shaper, and $C$ denotes the feedback controller for tracking control. Then, the closed-loop transfer function from reference to output can be expressed as

$$T(s) = \frac{C(s)IS(s)\tilde{P}(s)}{1 + C(s)IS(s)\tilde{P}(s)} = \frac{C(s)\tilde{P}(s)(A_1 + A_2 e^{-st_2})}{1 + C(s)\tilde{P}(s)(A_1 + A_2 e^{-st_2})} \tag{7}$$

Therefore, the characteristic equation of the closed-loop system is

$$1 + (A_1 + A_2 e^{-st_2})C(s)\tilde{P}(s) = 0 \tag{8}$$

As the ZV shaper has infinite number of zeros [23], the characteristic Eq. (8) has infinite number of solutions. Thus, the closed-loop system has infinite number of poles. This presents a potential closed-loop instability. Furthermore, the presence of the time delay makes the controller design more difficult. For these reasons, a Smith predictor is introduced in this work.

### 2.3. Smith predictor

The Smith predictor is a type of predictive controller for systems with time delays [39]. The typical structure for a linear dynamic system is illustrated in Fig. 6, where $P(s)e^{-s\tau}$ is the dynamic system with time delay, $P_m$ is the nominal model of $P(s)$, and $\tau_m$ is the estimated delay time. When $P(s) = P_m(s)$ and $\tau = \tau_m$, the resulting closed-loop transfer function from reference to output can be written as

$$T(s) = \frac{C(s)P(s)}{1 + C(s)P(s)} e^{-s\tau} \tag{9}$$

Obviously, the time delay term is removed from the characteristic equation of the closed-loop systems by the Smith predictor.

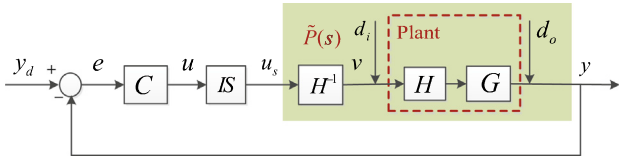


**Fig. 5.** The block diagram of feedback input shaping configuration with hysteresis compensation.

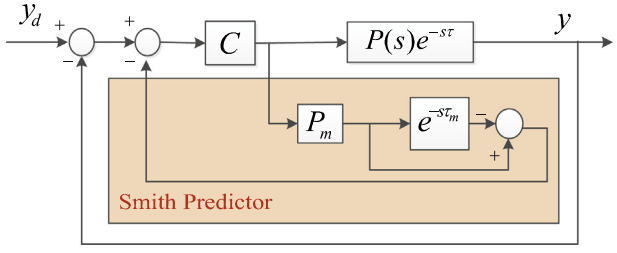


**Fig. 6.** The typical structure of Smith predictor.

Motivated by this idea, the Smith predictor is used to prevent the potential closed-loop instability caused by the time delays of the inside-the-loop input shaper. $P(s)$ and $e^{-s\tau}$ shown in Fig. 6 are replaced with the hysteresis compensated system $\tilde{P}(s)$ and the input shaper $IS$, respectively. The structure of the feedback input shaping controller with hysteresis compensation and Smith predictor is illustrated in Fig. 7. The transfer function from $e(t)$ to $u(t)$ is

$$C_m(s) = \frac{C(s)}{1 + C(s)C_s(s)} \tag{10}$$

where $C_s(s) = P_m(s)(1 - IS(s))$. Then, the closed-loop transfer function from reference to output can be expressed as

$$\begin{aligned} T(s) &= \frac{C_m(s)IS(s)\tilde{P}(s)}{1 + C_m(s)IS(s)\tilde{P}(s)} \\ &= \frac{C(s)IS(s)\tilde{P}(s)}{1 + C(s)P_m(s) - C(s)IS(s)(P_m(s) - \tilde{P}(s))} \end{aligned} \tag{11}$$

Thus, the characteristic equation of the closed-loop system is

$$1 + C(s)P_m(s) - C(s)IS(s)(P_m(s) - \tilde{P}(s)) = 0. \tag{12}$$

When $P_m = \tilde{P}(s)$, the transfer function $T(s)$ becomes

$$T(s) = \frac{C(s)\tilde{P}(s)}{1 + C(s)\tilde{P}(s)} IS(s) \tag{13}$$

and the characteristic Eq. (12) becomes

$$1 + C(s)\tilde{P}(s) = 0 \tag{14}$$

Comparing (14) with (8), it is observed that the term $A_1 + A_2 e^{-st_2}$ is removed from the characteristic equation. Therefore the potential closed-loop instability caused by the time delays of the inside-the-loop input shaper is prevented due to the inclusion of the Smith predictor.

### 2.4. Feedback controller

The foremost control objective in nanopositioning is to minimize the difference between the desired trajectory $y_d$ and the actual trajectory $y$. For this purpose, a high-gain PI type feedback controller is employed to mitigate the disturbances and modeling errors. The structure of the overall system is illustrated in Fig. 8, where $K_p$ and $K_i$ are the proportional gain and integral gain, respectively. In the following, the robust stability of the closed-loop system shall be analyzed for the plant with multiplicative uncertainties.

**Theorem 1** (*Robust Stability*). *Let the plant be modeled as* $\tilde{P}(s) = (1 + \Delta_p)P_m(s)$. *Assume that the nominal model* $P_m(s)$ *be minimum phase system, and a linear controller* $C(s)$ can stabilize $P_m(s)$. *Then a sufficient condition for robust stability of the closed-loop system for the uncertainty* $\Delta_p$ *is given as*

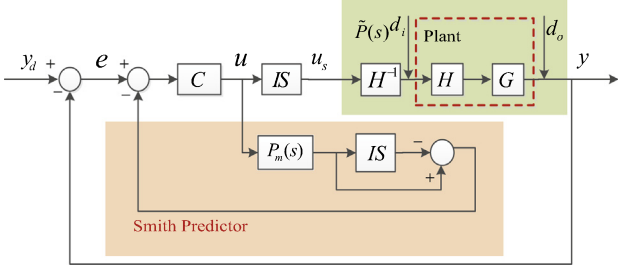


**Fig. 7.** The block diagram of the feedback input shaping configuration with hysteresis compensation and Smith predictor.

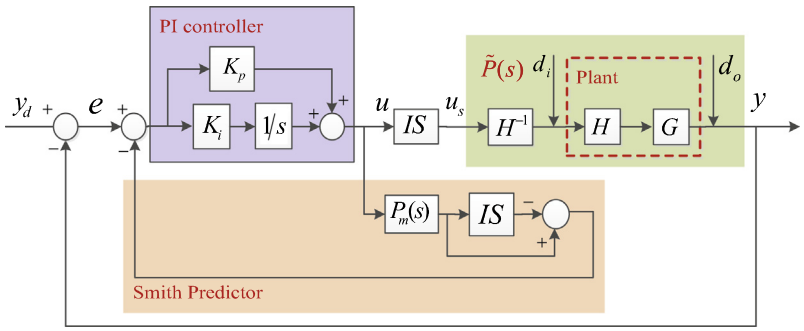


**Fig. 8.** The block diagram of the overall system.

$$|\Delta_p|_{s=j\omega} < \left|\frac{1+C(s)P_m(s)}{C(s)IS(s)P_m(s)}\right|_{s=j\omega}, \forall\omega \tag{15}$$

**Proof.** From (12), the characteristic polynomial of the closed-loop system $Q(s)$ can be expressed as

$$\begin{aligned} Q(s) &= 1 + C(s)P_m(s) - C(s)IS(s)(P_m(s) - \tilde{P}(s)) \\ &= 1 + C(s)P_m(s) + C(s)IS(s)P_m(s)\Delta_p \\ &= (1 + C(s)P_m(s))\left(1 + \frac{C(s)IS(s)P_m(s)}{1 + C(s)P_m(s)}\Delta_p\right) \end{aligned} \tag{16}$$

where $(1 + C(s)P_m(s))$ is stable by assumptions. After all, for the robust stability of the closed-loop system, the second term on the right-hand side in (16) must be stable. By *small gain theorem*, we can obtain

$$\left|\frac{C(s)IS(s)P_m(s)}{1 + C(s)P_m(s)}\Delta_p\right| < \left|\frac{C(s)IS(s)P_m(s)}{1 + C(s)P_m(s)}\right| \cdot |\Delta_p| < 1 \tag{17}$$

Then, (15) can be easily obtained from (17). □

## 3. Controller implementation

In this section, the control schemes discussed in Section 2 were implemented on a piezo-actuated nanopositioning stage.

### 3.1. Experimental setup

The experimental setup is shown in Fig. 9. The setup consists of a piezo-actuated stage, a dSPACE-DS1103 board, a high-voltage amplifier (HVA) and a position servo-control module (PSCM). The piezo-actuated stage is composed of a one-dimensional flexure hinge guiding mechanism, a preloaded piezoelectric stack actuator (PPSA), and a high-resolution strain gauge position sensor (SGPS). The PPSA (PSt 150/7/100 VS12, Piezomechanik, Germany) is used to drive the flexure mechanism with the maximum displacement of 75 μm. The SGPS integrated in the PPSA is used to measure the real-time displacement through the variance of the electrical resistance with the sensitivity of 0.148 V/μm, and a resolution of 2.07 nm. The dSPACE-DS1103 board (Germany), equipped with 16-bit DAC and 16-bit ADC, is employed to implement the control algorithms in the Matlab/Simulink environment on the computer. The DAC board sends the signal generated by the computer to the amplifier, which provides excitation voltage to the PPSA in the range of 0–150 V. The ADC board is used to capture the real-time displacement data, which is changed into analog voltage in the range of 0–10 V by the PSCM. The sampling frequency of the system is set to 20 kHz. The block diagram of the experiment setup is also shown in Fig. 9.

### 3.2. Hysteresis compensator

In order to construct the hysteresis compensator through (3), the parameters N, $a_1, a_2, r_i$ and $p_i$ should be obtained first. In this work, ten play operators are chosen for parameters identification

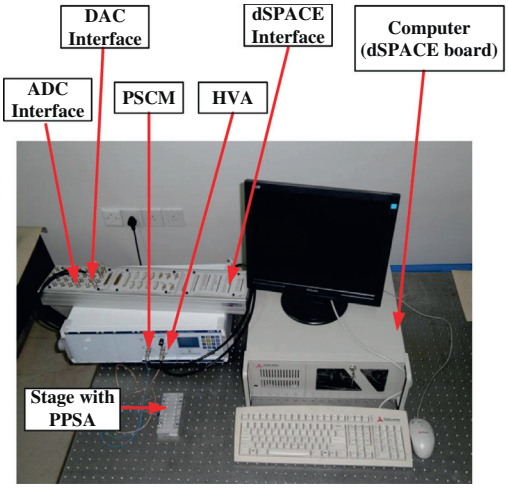


(a) Experimental platform

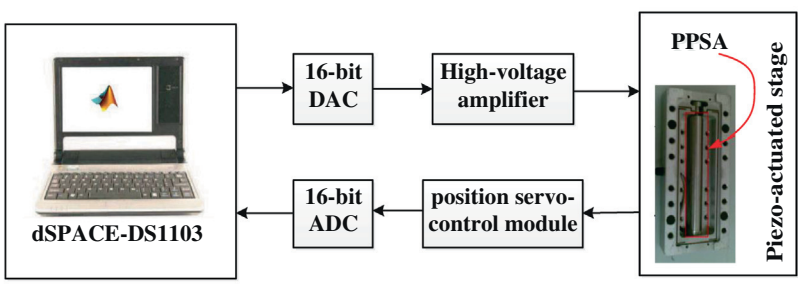


(b) Block diagram

**Fig. 9.** The experimental setup for tracking control of the piezo-actuated nanopositioning stage.

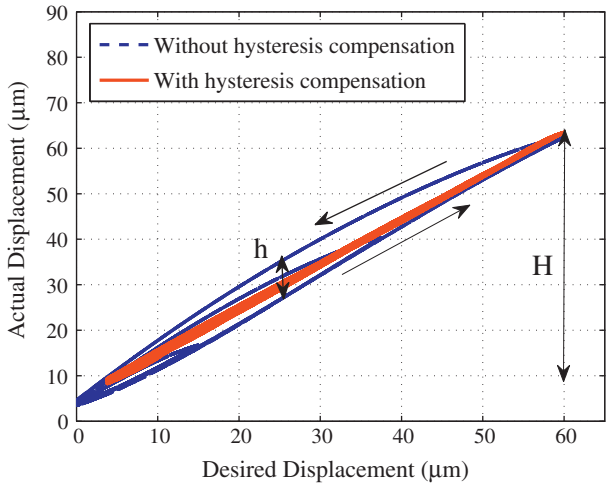


**Fig. 10.** Comparison of the results with and without hysteresis compensation.

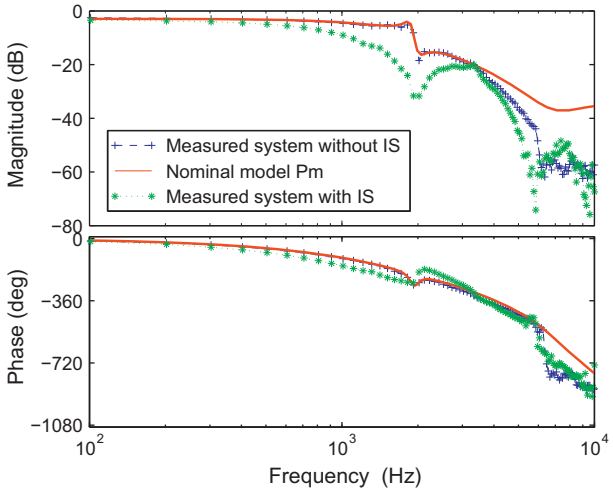


**Fig. 11.** The measured frequency responses of $\tilde{P}(s)$ and $\tilde{P}(s)IS(s)$ along with the simulated frequency response of the nominal model $P_m$.

and hysteresis compensation with fixed threshold values $r_i$ defined as

$$r_i = \frac{i}{N}\|y_d(t)\|_\infty, i = 0, 1, 2, \ldots, N-1 \tag{18}$$

with $\|y_d(t)\|_\infty = 1$in the normalized case. A multiple sine signal with different amplitudes and low-frequency components was used to excite the stage. The input signal and the displacement signal were simultaneously acquired by the dSPACE to be used as the identified signals. Then, the modified particle swarm optimization [35] was employed to identify other parameters $a_1, a_2$, and $p_i$.

With the identified parameters, the inverse hysteresis model was directly constructed through (3) and then implemented to compensate for the hysteresis nonlinearity. Fig. 10 shows the experimental results with a multi-amplitude triangular reference signal. It can be seen that the hysteresis width $((h/H) \times 100\%)$ has been reduced into 0.8% instead of 13.5% without hysteresis compensation. The results demonstrate the effectiveness of the direct inverse hysteresis compensation.

### 3.3. Input shaper

According to the discussion in Section 2.2, the design of the input shaper depends on the natural frequency and damping ratio of the linear dynamic system $\tilde{P}(s)$. Thus, a nominal model $P_m(s)$ of the system $\tilde{P}(s)$ should be identified first. Since the hysteresis nonlinearity has been compensated by the hysteresis compensator, a band-limited white noise signal is used to identify the model. The transfer function of $P_m(s)$, identified by the System Identification Toolbox of Matlab, can be expressed as:

$$P_m(s) = \frac{-0.017996(s - 1.214e005)(s^2 + 1095s + 1.568e008)(s^2 - 2.111e004s + 1.894e009)}{(s + 6.208e004)(s^2 + 1.7e004s + 1.053e008)(s^2 + 1005s + 1.393e008)} \tag{19}$$

Fig. 11 shows the frequency response of the hysteresis compensated system $\tilde{P}$ (from the input $u_s(t)$ to the output $y(t)$) along with the corresponding identified model $P_m$. The blue line in Fig. 11 refers to the experimental result of $\tilde{P}$, and the red line means the simulation result of the identified model $P_m$. It is demonstrated that the identified model captures the dynamics of the system with sufficient accuracy.

With the identified model (19), it is ready to design the input shaper for vibration damping. Analyzing the properties of the identified model (19), there are two resonance peaks at 1633 Hz and 1878 Hz, and the damping ratios at these two resonance peaks are 0.8283 and 0.0426, respectively. Therefore, the input shaper is designed to suppress the second resonance peak with a low damping ratio at 1878 Hz. According to (5) and (6), the input shaper can be written as:

$$IS(s) = 0.5334 + 0.4666e^{-2.6641e-04s}. \tag{20}$$

**Remark 2.** The zero vibration shaper in our work is derived and implemented in continuous time as the controller design is based on the dSPACE. In fact, it is expressed by the exponential transfer function, which can be approximated by a rational transfer function using Padé approximation formulas. If one wants to transform it to the discrete domain, the command c2d in matlab can be used. Generally, the delay time of the shaper is approximated to the nearest multiple times of the sampling time. However, if the sampling rate is not a lot higher than the vibration rate, then digital input shapers will be needed. The techniques to compute digital input shapers can be roughly classified into the following three categories: (1) Numerical conversion of continuous-input shapers to digital input shapers; (2) Z-plane zero placement techniques; (3) Direct solution of the vibration equations in the discrete time domain [40].

In order to validate the effect of the input shaper, a step reference signal was used to excite the systems with and without the input shaper. The results are shown in Fig. 12. It can be seen that the vibration level and settling time of the system with the input shaper are reduced a lot compared to those of the system without input shaper. Moreover, the results show that there exists a steady error under the open-loop structure.

Next, a frequency response test was performed in order to evaluate the performances more accurately. The result is given in

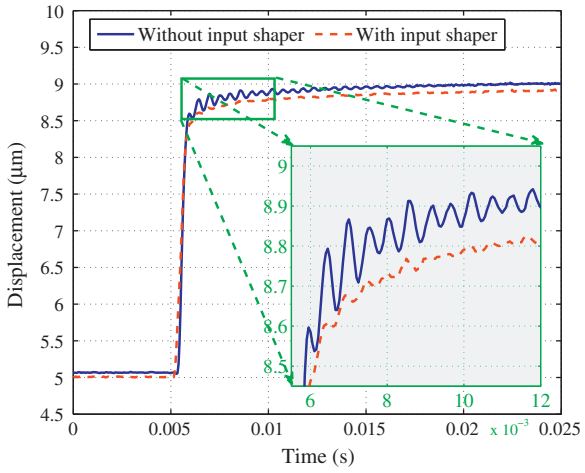


**Fig. 12.** Step response of the system with and without the input shaper.

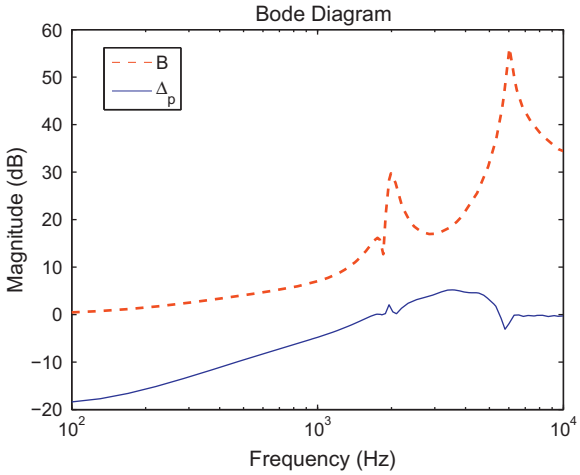


**Fig. 13.** The robust stability condition verification: the bode plot of the model uncertainty $\Delta_p$ and the calculated bound $B$.

Fig. 11. From the figure, we can see that the resonance peak is reduced from −5.27 dB to −24.2 dB due to the introduction of the input shaper. It indicates a significant increase of gain margin such that the feedback controller with high control gains is possible to be implemented to increase the tracking bandwidth of the system. This is in agreement with the conclusion obtained by [41].

### 3.4. Feedback controller

The parameters of the PI feedback controller, i.e. the proportional gain $K_p$ and integral gain $K_i$, are initially selected by the Matlab PID auto tuner, and then tuned by the trial and error method in the experiments. Table 1 lists the values of $K_p$ and $K_i$ in different controllers. The gain margin and phase margin are also given in the table. For the methods PI and PI+HC, the $K_p$ and $K_i$ are firstly selected as 0.7 and 1000 to obtain a large gain margin and low overshoot. Then the PI+HC is redesigned to maximize the tracking bandwidth, where the $K_p$ and $K_i$ are restricted to 1.2 and 3500 by the gain margin of only 2.37 dB. When the input shaper is placed inside the feedback loop, the gain margins are increased as indicated in the table, which are 12.7 and 14 dB for the PI+HC+IS and PI+HC+IS+SP, respectively.

Finally, the robust stability condition in Theorem 1 is verified. Fig. 13 shows the model uncertainty $\Delta_p$ and the calculated bound $B$, where $\Delta_p = (\tilde{P} - P_m)P_m^{-1}$, and $B = \left|\frac{1+CP_m}{CP_mIS}\right|$. Note that the model uncertainty curve is below the calculated bound curve at all the frequency range. Therefore, the robust stability condition is satisfied for the closed-loop system as presented in the Theorem 1.

## 4. Experimental results

The controllers developed above are experimentally evaluated with the following tests: (1) Step signal – the most common signal to evaluate the controller performance in time domain (i.e., rising time, settling time, overshoot) and test the point-to-point tracking performance; (2) Sinusoidal signal – the most general continuous trajectory in positioning applications used to test the tracking performance; (3) Band-limited white noise signal – the widely used signal to measure the frequency response of the system; (4) Impulse signal – a signal similar to the disturbance that affects the real device, such as the sudden change.

During these tests, the components of the controllers are sequentially included in four combinations: (1) PI controller (PI); (2) PI controller + hysteresis compensator (PI+HC); (3) PI controller + hysteresis compensator + input shaper (PI+HC+IS); (4) PI controller + hysteresis compensator + input shaper + Smith predictor (PI+HC+IS+SP).

**Table 1**
Control parameters and performance of different controllers.

| | PI | PI+HC | | PI+HC+IS | PI+HC+IS+SP |
|---|---|---|---|---|---|
| $C(s)$ | $\frac{0.7s+1000}{s}$ | $\frac{0.7s+1000}{s}$ | $\frac{1.2s+3500}{s}$ | $\frac{1.2s+3500}{s}$ | $\frac{1.2s+3500}{s}$ |
| $gm$ | 9.41 | 7.72 | 2.37 | 12.7 | 14 |
| $pm$ | 102° | 111° | 98.5° | 77.9° | 88° |
| $t_r$ (ms) | 3.2384 | 2.8537 | 0.3074 | 0.4854 | 0.6173 |
| $t_s$ (ms) | 5.7508 | 5.1803 | 5.6786 | 2.8638 | 0.8629 |
| $N_v$ | 0 | 0 | 7.5 | 2 | 0.5 |
| $M_p$ | 0 | 0 | 32.91% | 42.73% | 4.22% |

### 4.1. Experimental results using step signals

In this section, a step signal is used to test the transient responses of the different controllers. The experimental results are shown in Fig. 14. For a quantitative comparison, some performance indexes are summarized in Table 1, where $t_r$ is the rising time, $t_s$ is the 2% settling time, $M_p$ is the overshoot, and $N_v$ is the number of vibration, defined as half of the number that the response curve passes through the steady value. A small $t_r$ and $t_s$ indicate the quick

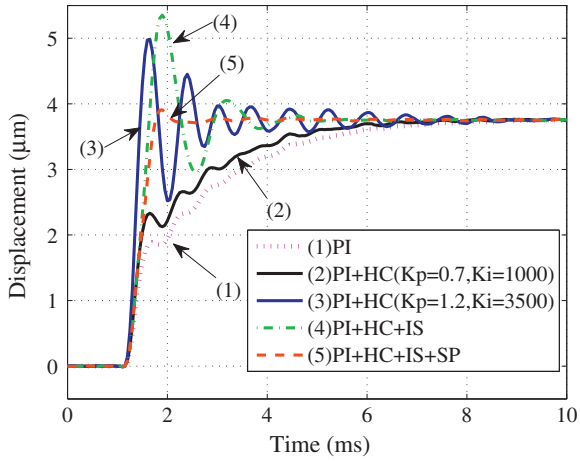


**Fig. 14.** Comparison of the step responses using different control methods.

response speed, and a small $M_p$ and $N_v$ indicate the large damping ratio. For the PI and PI+HC (curve (1)(2) in Fig. 14), the $M_p$ and $N_v$ are zero, however, the $t_r$ and $t_s$ are large, which indicates the response speed is too slow. In order to improve this, the $K_p$ and $K_i$ of the PI+HC are increased to 1.2 and 3500, then the $t_r$ of the step response (curve (3) in Fig. 14) are reduced from 2.8537 to 0.3074 ms. However, the $t_s$ is increased from 5.1803 to 5.6786 ms, $N_v$ and $M_p$ are increased to 7.5 and 32.91% respectively. When the inside-the-loop input shaper is included, the settling time $t_s$ of the step response (curve (4) in Fig. 14) is reduced to 2.8638 ms, about 49% improvement compared to PI+HC (curve (3)). Moreover, the $N_v$ is also reduced from 7.5 to 2. However, a significantly large overshoot is observed from curve (4), which is about 42.73%. This is because the PI+HC+IS is more likely to result in a limit cycle response, even the instability [23]. In this paper, a Smith predictor is adopted to overcome this problem. The step response of the PI+HC+IS+SP is shown in Fig. 14 (curve (5)). Compared with curve (4), the $M_p$ of the curve (5) is significantly reduced, from 42.73% to 4.22%, which indicates an improvement of 90%. Furthermore, the $t_s$ and $N_v$ are also reduced to 0.8629 ms and 0.5 respectively, whereas the rising time $t_r$ is slightly increased to 0.6173 ms. Hence, conclusion can be drawn that the proposed controller PI+HC+IS+SP is significantly better than other listed controllers in terms of settling time, number of vibration, and overshoot.

### 4.2. Experimental results using sinusoidal signals

In this section, the sinusoidal signals with fixed amplitude (7.5 μm) and different frequencies (10 Hz, 50 Hz, and 100 Hz) are used to test the tracking performance of the proposed control method. Firstly, a performance index is chosen for a quantitative comparison. When discussing the tracking performance in SPM applications, perfectly delayed tracking is better than imperfect timely tracking if we know the delay well. According to the reference [42], the following two performance indexes shall be used in this work for the comparative study:

$$J_m = \max_{t\in[t_{ss},t_{ss}+2T)} |y(t) - y_d(t - k^* T_s)| \tag{21}$$

$$J_e = \sqrt{\frac{1}{2T}\int_{t_{ss}}^{t_{ss}+2T} (y(t) - y_d(t - k^* T_s))^2 dt} \tag{22}$$

**Table 2**
Tracking performance of different controllers under sinusoidal signals with variant frequencies.

| | | PI | PI+HC | PI+HC+IS | PI+HC+IS+SP |
|---|---|---|---|---|---|
| 10 Hz | $J_m$ (μm) | 0.3406 | 0.2706 | 0.0413 | 0.0344 |
| | $J_e$ (μm) | 0.2301 | 0.1824 | 0.0138 | 0.0120 |
| 50 Hz | $J_m$ (μm) | 1.5371 | 1.2376 | 0.0769 | 0.0667 |
| | $J_e$ (μm) | 1.0674 | 0.8627 | 0.0373 | 0.0351 |
| 100 Hz | $J_m$ (μm) | 2.3667 | 2.0168 | 0.1062 | 0.0998 |
| | $J_e$ (μm) | 1.6599 | 1.4209 | 0.0617 | 0.0569 |

where $T$ is the period of the sinusoidal signal, $T_s = 50\mu s$ is the controller sampling period, $t_{ss}$ is the time at which all transients have died out, $y(t)$ is the actual output, $y_d(t)$ is the desired input, $y_d(t - k^* T_s)$ is the shifted input, and the variable $k^*$ is defined as

$$k^* = \arg\min_k \max_{t\in[t_{ss},t_{ss}+NT)} |y(t) - y_d(t - kT_s)| \tag{23}$$

where $k$ is a variable defined on $[0, T/T_s]$, and $N$ is the number of recorded periods after transients have died output.

The tracking errors is provided in Fig. 15, which is defined as $y(t) - y_d(t - k^* T_s)$ for PI+HC+IS and PI+HC+IS+SP methods, while $y(t) - y_d(t)$ for PI and PI+HC methods. From the figure, we can see that the tracking performance of the closed-loop systems with input shaper is superior to the systems without input shaper. This is further evidenced in Table 2, which summaries the two error indexes $J_m$ and $J_e$ defined in (21) and (22). As observed in the table, the introduction of the input shaper results in a significant improvement of 85–95% compared to that without input shaper. The Smith predictor further improve the tracking performance by 6–16%. The percentages of improvement indicated above are calculated by

$$\left(1 - \frac{e_a}{e_b}\right) \times 100\% \tag{24}$$

with $e_a$ and $e_b$ being the error indexes, i.e., $J_m$ or $J_e$, of the controllers $a$ and $b$, respectively.

### 4.3. Experimental results using band-limit white noise signals

A band-limit white noise signal is used to test the closed-loop frequency responses of the developed controllers. The results are shown in Fig. 16. The −3 dB control bandwidth of the controllers

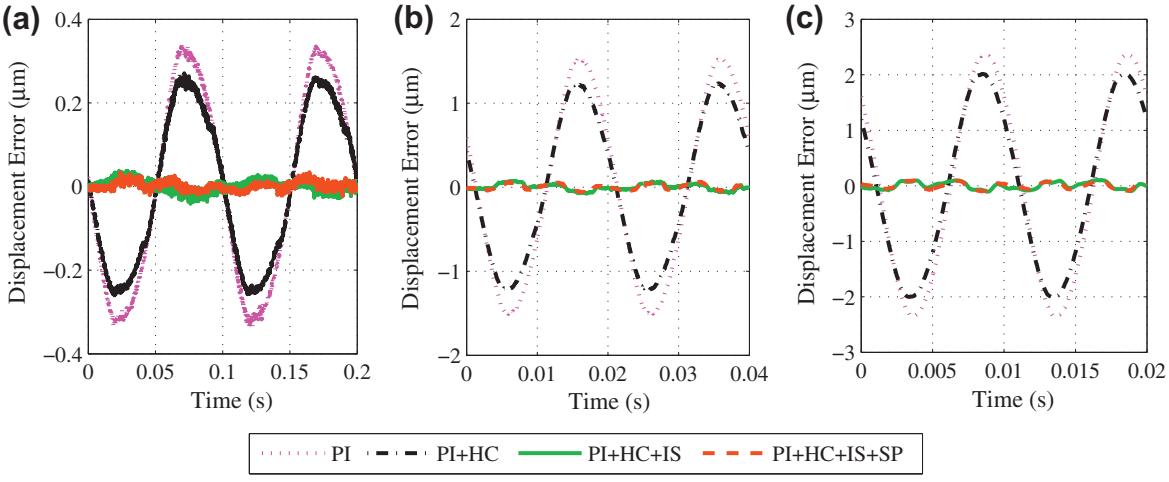


**Fig. 15.** Comparison of the tracking error by using PI, PI+HC, PI+HC+IS, and PI+HC+IS+SP methods for sinusoidal signals with different frequencies of (a) 10 Hz, (b) 50 Hz, and (c) 100 Hz. The tracking error is defined as $y(t) - y_d(t - k^* T_s)$ for PI+HC+IS and PI+HC+IS+SP methods, while $y(t) - y_d(t)$ for PI and PI+HC methods.

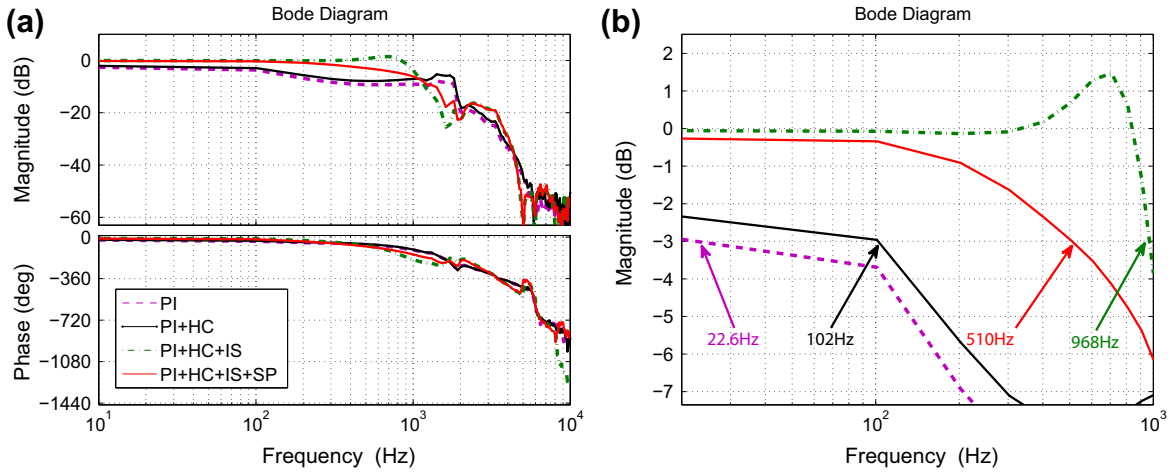


**Fig. 16.** Comparison of the closed-loop transfer functions with the various control methods: (a) full view; (b) a zoomed-in view.

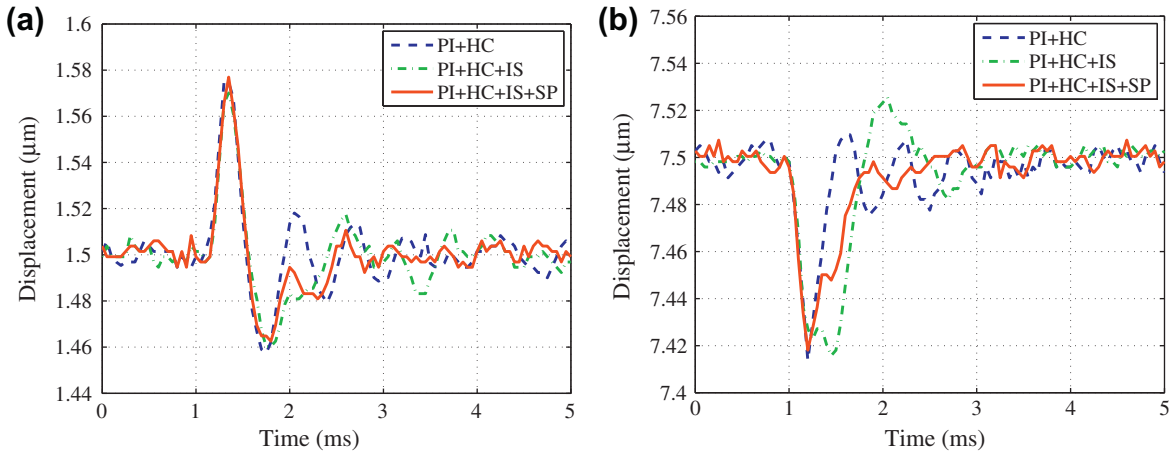


**Fig. 17.** Comparison of disturbance responses with different controllers: (a) input disturbance; (b) output disturbance.

are also given in the zoomed-in view. As observed, the introduction of hysteresis compensator increases the control bandwidth from 22.6 Hz to 102 Hz. The implementation of input shaper increases the control bandwidth to 968 Hz, however, some of the bandwidth are uncontrollable. The proposed approach PI+HC+IS+SP achieves the control bandwidth of 510 Hz, all of which are controllable. Compared to the system with PI+HC control approach, the proposed controller increases the control bandwidth by 5 times.

### *4.4. Experimental results using impulse signals*

In this section, an impulse signal is used as disturbance to test the disturbance rejection capabilities of different controllers. Fig. 17(a) shows the responses to the input disturbance (actuator disturbance), and Fig. 17(b) shows the responses to the output disturbance (sensor disturbance). From the figure, it is demonstrated that the PI+HC+IS+SP controller is capable of reducing oscillation caused by disturbances. Moreover, it is revealed that the proposed PI+HC+IS+SP can reject both the input disturbance and the output disturbance more effectively than the PI+HC and the PI+HC+IS.

## 5. Conclusion

In this paper, a high-bandwidth controller is proposed for the piezo-actuated nanopositioning stage. Firstly, a direct inverse hysteresis model, which is characterized by a modified P-I model, is designed to compensate for the hysteresis nonlinearity. The result shows that the hysteresis has been reduced into 0.8% instead of 13.5% without hysteresis compensation. Then, an inside-the-loop input shaper is developed for vibration damping of the hysteresis compensated system. It reduces the resonance peak from −5.27 dB to −24.2 dB, enabling the implementation of the high-gain feedback controller. A Smith predictor is included in the feedback loop to prevent the potential closed-loop instability caused by the delays of the inside-the-loop input shaper. Finally, a high-gain PI feedback controller is employed to handle the disturbances and modeling uncertainty. A series of comparative experiments are performed on a piezo-actuated nanopositioning stage to verify the effectiveness of the propose approach under different test signals. With the proposed method, the bandwidth of the piezo-actuated stages is increased from 22.6 Hz (only with PI controller) to 510 Hz.

## Acknowledgment

This work was supported by the National Natural Science Foundation of China (Grant No. 91023047), the Shu Guang project supported by Shanghai Municipal Education Commission (Grant No. 10SG17), and Specialized Research Fund for the Doctoral Program of Higher Education (Grant No. 20130073110037).

## References


[1] Salapaka S, Salapaka M. Scanning probe microscopy. IEEE Control Syst 2008;28(2):65–83.
[2] Tian Y, Zhang D, Shirinzadeh B. Dynamic modelling of a flexure-based mechanism for ultra-precision grinding operation. Precis Eng 2011;35(4):554–65.
[3] Yong Y, Moheimani S, Kenton B, Leang K. Invited review article: High-speed flexure-guided nanopositioning: mechanical design and control issues. Rev Sci Instrum 2012;83:121101.
[4] Gu G, Zhu L. Motion control of piezoceramic actuators with creep, hysteresis and vibration compensation. Sens Actuat A: Phys 2013;197:76–87.
[5] Jordan S. Eliminating vibration in the nano-world. Photon Spectra 2002;36:60–72.
[6] Singer NC, Seering WP. Preshaping command inputs to reduce system vibration. ASME Trans J Dynam Syst Measur Control 1990;112:76–82.
[7] Smith OJM. Feedback control systems. New York: McGraw-Hill; 1958.
[8] Gu G, Zhu L, Su C. Integral resonant damping for high-bandwidth control of piezoceramic stack actuators with asymmetric hysteresis nonlinearity. Mechatronics 2014;24(4):367–75.
[9] Mahmood I, Moheimani S. Making a commercial atomic force microscope more accurate and faster using positive position feedback control. Rev Sci Instrum 2009;80:063705.
[10] Singhose W, Singer N, Seering W. Time-optimal negative input shapers. ASME Trans J Dynam Syst Measur Control 1997;119:198–205.
[11] Schitter G, Thurner P, Hansma P. Design and input-shaping control of a novel scanner for high-speed atomic force microscopy. Mechatronics 2008;18:282–8.
[12] Khorrami F, Jain S, Tzes A. Experiments of rigid-body based controllers with input preshaping for a two-link flexible manipulator. In: American control conference, Chicago, IL; 1992. p. 2957–61.
[13] Zuo K, Wang D. Closed-loop shaped-input control of a class of manipulators with a single flexible link. In: IEEE international conference on robotics and automation, Nice, France; 1992. p. 782–7.
[14] Tzes A, Yurkovich S. An adaptive input shaping control scheme for vibration suppression in slewing flexible structures. IEEE Trans Control Syst Technol 1993;1:114–21.
[15] Zain M, Tokhi M, Mohamed Z. Hybrid learning control schemes with input shaping of a flexible manipulator system. Mechatronics 2006;16:209–19.
[16] Singh T, Vadali SR. Input-shaped control of three-dimensional maneuvers of flexible spacecraft. J Guid Control Dynam 1993;16:1061–8.
[17] Singhose W, Singer N, Seering W. Vibration reduction in 0-g using input shaping on the MIT middeck active control experiment. In: American control conference, Seattle, WA; 1995. p. 919–23.
[18] Singhose W, Porter LJ, Tuttle TD, Singer NC. Vibration reduction using multi-hump input shapers. ASME Trans J Dynam Syst Measur Control 1997;119:320–6.
[19] Singhose W, Porter L, Kenison M, Kriikku E. Effects of hoisting on the input shaping control of gantry cranes. Control Eng Pract 2000;8(10):1159–65.
[20] Sorensen K, Singhose W, Dickerson S. A controller enabling precise positioning and sway reduction in bridge and gantry cranes. Control Eng Pract 2007;15(7):825–37.
[21] Kapila V, Tzes A, Yan Q. Closed-loop input shaping for flexible structures using time-delay control. ASME Trans J Dynam Syst Measur Control 2000;122:454–60.
[22] Huey JR, Sorensen KL, Singhose WE. Useful applications of closed-loop signal shaping controllers. Control Eng Pract 2008;16:836–46.
[23] Huey JR, Singhose W. Trends in the stability properties of CLSS controllers: a root-locus analysis. IEEE Trans Control Syst Technol 2010;18:1044–56.
[24] Staehlin U, Singh T, Design of closed-loop input shaping controllers. In: Proceedings of the 2003 American control conference, vol. 6; 2003. p. 5167–72.
[25] Hung J. Feedback control with posicast. IEEE Trans Indust Electron 2002;50(1):94–9.
[26] Kucera V, Hromcik M. Delay-based input shapers in feedback interconnections. In: Proceedings of the 18th IFAC world congress, Milan; 2011. p. 7577–82.
[27] Clayton G, Tien S, Fleming A, Moheimani S, Devasia S. Inverse-feedforward of charge-controlled piezopositioners. Mechatronics 2008;18:273–81.
[28] Chen X, Hisayam T. Adaptive sliding-mode position control for piezo-actuated stage. IEEE Trans Indust Electron 2008;55(11):3927–34.
[29] Lin C, Lin P. Particle swarm optimization based feedforward controller for a XY PZT positioning stage. Mechatronics 2012;22(5):614–28.
[30] Kuhnen K. Modeling, identification and compensation of complex hysteretic nonlinearities: a modified Prandtl-Ishlinskii approach. Eur J Control 2003;9(4):407–18.
[31] Gu G, Zhu L, Su C. Modeling and compensation of asymmetric hysteresis nonlinearity for piezoceramic actuators with a modified Prandtl-Ishlinskii model. IEEE Trans Indust Electron 2014;61(3):1583–95.
[32] Hu H, Mrad R. On the classical Preisach model for hysteresis in piezoceramic actuators. Mechatronics 2002;13(2):85–94.
[33] Gu G, Yang M, Zhu L. Real-time inverse hysteresis compensation of piezoelectric actuators with a modified Prandtl-Ishlinskii model. Rev Sci Instrum 2012;83:065106.
[34] Boukari A, Carmona J, Moraru G, Malburet F, Chaaba A, Douimi M. Piezo-actuators modeling for smart applications. Mechatronics 2011;21:339–49.
[35] Yang M, Gu G, Zhu L. Parameter identification of the generalized Prandtl-Ishlinskii model for piezoelectric actuators using modified particle swarm optimization. Sens Actuat A: Phys 2013;189:254–65.
[36] Singh T, Singhose W. Tutorial on input shaping/time delay control of maneuvering flexible structures. In: Proceedings of the American control conference, Anchorage, AK; 2002. p. 1717–31.
[37] Singhose W. Command shaping for flexible systems: a review of the first 50 years. Int J Precis Eng Manuf 2009;10(4):153–68.
[38] Singhose W, Vaughan J. Reducing vibration by digital filtering and input shaping. IEEE Trans Control Syst Technol 2011;19(6):1410–20.
[39] Abe N, Yamanaka K. Smith predictor control and internal model control – a tutorial –. In: SICE annual conference 2003, Fukui, Japan; 2003. p. 1383–7.
[40] Robertson M, Kozak K, Singhose W. Computational framework for digital input shapers using linear optimisation. IEE Proc – Control Theory Appl 2006;153(3):314–22.
[41] Kenison M, Singhose W. Concurrent design of input shaping and proportional plus derivative feedback control. ASME Trans J Dynam Syst Measur Control 2002;124:398–405.
[42] Butterworth J, Pao L, Abramovitch D. A discrete-time single-parameter combined feedforward/feedback adaptive-delay algorithm with applications to piezo-based raster tracking. IEEE Trans Control Syst Technol 2012;20(2):416–23.